Tampuu, Tauri; Praks, Jaan; Kull, Ain; Uiboupin, Rivo; Tamm, Tanel; Voormansik, Kaupo

Detecting peat extraction related activity with multi-temporal Sentinel-1 InSAR coherence time series

Published in:
International Journal of Applied Earth Observation and Geoinformation

DOI:
10.1016/j.jag.2021.102309

Published: 01/06/2021

Document Version
Publisher's PDF, also known as Version of record

International Journal of Applied Earth Observations and Geoinformation 98 (2021) 102309

Contents lists available at ScienceDirect

International Journal of Applied Earth Observations and Geoinformation

journal homepage: www.elsevier.com/locate/jag

Detecting peat extraction related activity with multi-temporal Sentinel-1 InSAR coherence time series

Tauri Tampuu[a,*], Jaan Praks[b], Ain Kull[a], Rivo Uiboupin[c], Tanel Tamm[d], Kaupo Voormansik[d,e]

[a] *Institute of Ecology and Earth Sciences, University of Tartu, 46 Vanemuise St., Tartu 51014, Estonia*
[b] *School of Electrical Engineering, Aalto University, Maarintie 8, 02150 Espoo, Finland*
[c] *Department of Marine Systems, Tallinn University of Technology, Akadeemia Rd. 15a, Tallinn 12618, Estonia*
[d] *KappaZeta Ltd., 52-4 Herne St., Tartu 51007, Estonia*
[e] *Tartu Observatory, University of Tartu, Observatooriumi 1, Tõravere 61602, Estonia*

ARTICLE INFO

Keywords:
Bog
SAR interferometry
Coherence
Peatland
Change detection
Monitoring

ABSTRACT

Monitoring of when, where and in which quantity peat is harvested is currently based on manual declarations. Synthetic Aperture Radar (SAR) is a powerful tool for change detection and monitoring. The aim of this study was to evaluate whether Sentinel-1 6-day interferometric SAR (InSAR) temporal coherence could allow peat extraction monitoring from satellite. We demonstrate that temporal median coherence enables to detect harvest related surface altering works and therefore also spatially explicitly determine active and inactive extraction areas. A polygon-based multi-orbit time series approach is sufficient for the task. Hereby, vertical–vertical polarisation (VV) is more sensitive to the changes compared to vertical-horizontal (VH). During the main harvest season the peat extraction area has median VV coherence lower than 0.2 while the abandoned area and open bog which serve as reference for undisturbed extraction area have close to 0.6. Also, the potential for coherence based milled peat extraction intensity estimation is demonstrated and an indication is given how partially extracted areas could be distinguished from fully harvested and not harvest areas, by the use of coherence standard deviation. Regarding the influence of rainfall, only heavy rain on one of the acquisitions of the image pair whereas the other is from dry conditions seems to cause decorrelation comparable to surface altering works. Moreover, deploying images from multiple consecutive orbits or introducing backscatter intensity σ^0 or reference polygons of undisturbed area helps to reduce risk for rain induced false positives. Developing an operational algorithm for peat extraction identification could be undertaken in future studies.

1. Introduction

Peatlands store about 20–30% of the global soil carbon while covering only ~3% of the land surface (Gorham, 1991; Yu et al., 2010; Köchy et al., 2015; Leifeld and Menichetti, 2018). This is more than half of the current atmospheric carbon (Drösler et al., 2008), equivalent to the carbon of all terrestrial biomass, and twice the carbon contained in all the forest biomass (Parish et al., 2008). The major fraction of all peatlands is found in northern temperate and cold climates (Parish et al., 2008). Peatlands are naturally sinks of carbon but they may switch from a net sequesterer to emitter of greenhouse gases (GHG) resulting from changes in the water regime which is highly vulnerable both to climatic changes and direct human impact (Gorham, 1991; Ojanen et al., 2010; Yu, 2012; Webster et al., 2018). Consequently, active and abandoned peat extraction sites are persistent sources of GHG (Waddington et al., 2009; Salm et al., 2012; Beyer and Höper, 2015; Mustamo et al., 2016).

Monitoring and control of peat extraction activities is an increasingly important topic with global importance in the context of GHG emissions, habitat loss and water quality (Chapman et al., 2003; Drösler et al., 2008; Tuukkanen et al., 2017). In this paper we evaluate the applicability of spaceborne InSAR time series in monitoring peatland harvesting activities in northern peatlands. Our approach is based on the assumption that a peat extraction area displays high coherence until a surface altering event takes place, which causes a sudden significant loss in coherence. Natural peatlands have been investigated in Tampuu et al. (2020) where we showed that open bogs retain high coherence even over several months. InSAR coherence has already been used to detect prompt surface altering events (Wegmüller and Werner, 1995). Forest

* Corresponding author.
E-mail address: tauri.tampuu@ut.ee (T. Tampuu).

https://doi.org/10.1016/j.jag.2021.102309
Received 30 December 2019; Received in revised form 31 July 2020; Accepted 20 January 2021
Available online 8 February 2021

clear-cuts are detectable (Smith and Askne, 2001), ploughing, tillage and harvesting cause complete decorrelation in farmed areas, whereas the post-harvest bare or stubble field is identifiable by high correlation (Wegmüller and Werner, 1997). Tamm et al. (2016) presented a proof of concept for detecting mowing events on agricultural grasslands. The main challenge of the method is related to changing weather conditions which also cause decorrelation (Askne et al., 1997; Askne et al., 2003). Especially, rainfall can remarkably decrease coherence in grasslands (Tamm et al., 2016) and even completely decorrelate the entire scene consisting of various land cover classes such as open land, cultivated land, forests, clearcuts, marshes and urban areas (Santoro et al., 2002). Furthermore, the effect of soil moisture changes on the coherence over a bare agricultural soil (De Zan et al., 2014) and in arid lands (Scott et al., 2017) has been demonstrated.

Currently there are limited tools to monitor peat harvesting with sufficient temporal frequency and authorities rely solely on producers' reports. The aim of this study is to demonstrate that Sentinel-1 6-day InSAR coherence allows to: 1) distinguish active peat extraction sites from abandoned sites; 2) detect activities associated to peat extraction; 3) distinguish between partially and fully harvested blocks. That would enable to monitor peat production by an independent party and manage the production spatially more explicitly to ensure sustainable use of resources. The depletion of a production block is desired for the climate change mitigation and restoration. Contrary, harvesting only the uppermost least decomposed peat layers and thereafter opening a new block is more profitable.

2. Materials and methods

2.1. Study area and in situ data

The study covers three peat harvesting sites in Central Estonia: Sangla (58°20′ N, 26°14′ E), Soosaare (58°33′ N, 25°53′ E) and Tässi bogs (58°32′ N, 25°51′ E) (Fig. 1). While Tässi bog has been entirely converted to a peat extraction site, in the Soosaare and Sangla bogs significant parts are still undrained and serve as natural references for the same peat production sites. Soosaare and Tässi extraction sites both consist of 8 production blocks (a peat extraction site is divided into blocks by a road network; a block consists of ~20 m wide extraction fields, divided by ditches). The Soosaare and Tässi dataset consists of a list of harvesting events with the measure of areal cover of performed work (as sometimes a block is harvested only partly) with a day precision for each block. The dataset covers the period of May 11–August 3, 2018. In the Sangla extraction site, data are available for 2 blocks. The Sangla dataset covers a full milled peat harvest cycle related works (milling, turning, harvesting) in a day precision for both blocks. An areal measure of performed work is not included. The Sangla dataset covers the period of May 8–July 27, 2018. Minor inconsistencies exist because the datasets originate from two different peat producers, based on their own reporting procedures. However, we had no record of the maintenance works not directly connected to harvesting (e.g. field profiling, ditch maintenance), complicating interpretation of the satellite data beyond the main harvesting season.

2.2. Peat extraction

In the study sites, milled peat is harvested by the Haku method or the pneumatic extraction technique (Tissari et al., 2006). The harvest cycle consists of 3 stages. First, the upper layer of peat is milled to the depth of 10–20 mm, then the milled fields are left to be dried by air till the humidity content has dropped to around 40% (Cleary et al., 2005; Eesti Turbaliit, 2019). During drying, the peat is turned to ensure faster and more even drying. Turning is performed 1–3 times, drying takes 2–3 days. In the case of rain, the process has to be repeated. Eventually, the harvesting is performed and the harvested peat is stockpiled at the end of the field until utilisation (Sundh et al., 2000; Eesti Turbaliit, 2019). Such production cycles are repeated 10–15 times during the season, depending on the weather (harvesting is directly affected by the sunshine, temperature, wind and rain) and characteristics of the peat deposit (Eesti Turbaliit, 2019).

The peat extraction season in Estonia lasts usually from May to August with the peak time of harvesting in June and July (Pakere and Blumberga, 2017; Eesti Turbaliit, 2019). However, peat extraction contains also routine maintenance works not directly connected to harvesting (Graf et al., 2012). Those works are often carried out before or after the main harvesting period, though they can also be performed

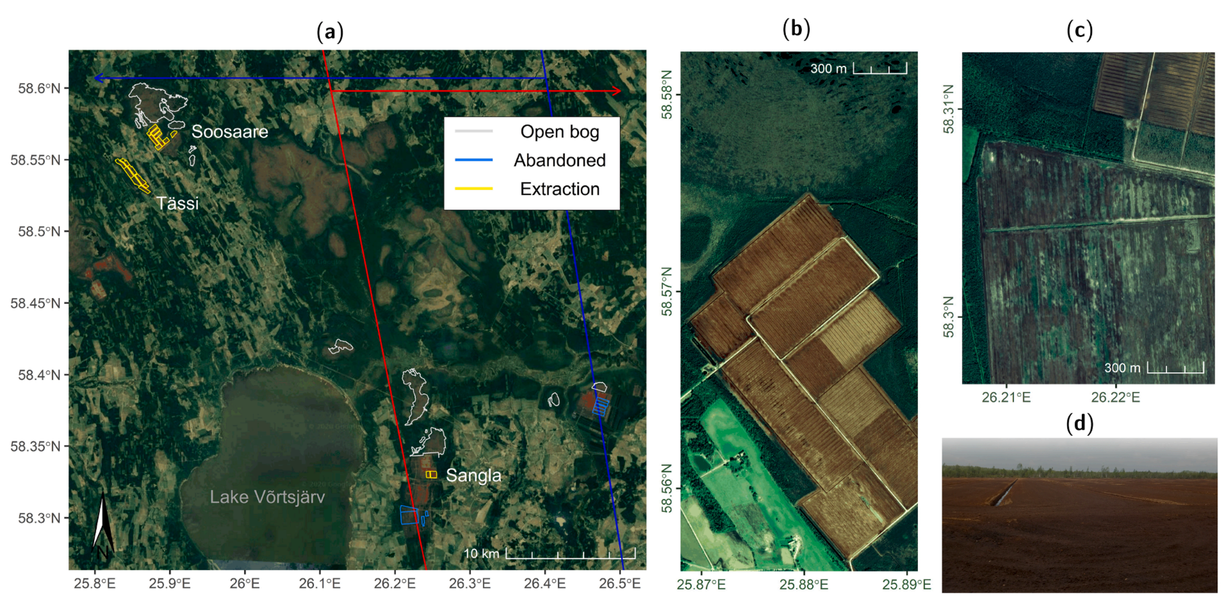

Fig. 1. The study area and the approximate coverage of the Sentinel-1 orbits denoted by RONs. RON 87 covers the eastern side of the scene (indicated by red line with an arrow), RON 58 covers the western side (indicated by blue line), RON 160 covers the entire scene. Yellow polygons mark peat production (extraction) blocks, gray the open bog and blue abandoned sites (a). The areal images cover extraction blocks and the natural open bog in Soosaare bog (b), and the abandoned area and extraction blocks (upper right corner of the image) in Sangla bog (c). The photograph looks over the extraction area in Sangla bog (d). (For interpretation of the references to colour in this figure legend, the reader is referred to the web version of this article.)

simultaneously with harvesting.

2.3. Precipitation

Natural conditions cause decorrelation between SAR images which might significantly affect the analysis. Therefore, the summarised daily precipitation data from the Estonian Weather Service (Estonian Environment Agency, 2020) are included to the analysis. For the Soosaare and Tässi sites, we derived the rainfall estimates as the average from the three closest meteorological stations (Viljandi, 25 km; Türi, 38 km and; Jõgeva, 35 km) surrounding the sites. The rainfall data for the Sangla site are from the Tartu-Tõravere station (14 km to SE). Based on the summarised daily precipitation values, we also computed the accumulated rainfall estimate for a 3-day period preceding a Sentinel-1 acquisition.

2.4. SAR data

The C-band SAR satellite Sentinel-1 Interferometric Wide swath mode (IW) Single Look Complex (SLC) dual-pol data products are used: vertical transmit – horizontal receive (cross-polarisation VH) and vertical transmit – vertical receive (co-polarisation VV). Combination of Sentinel-1A and Sentinel-1B enables to produce small baseline interferometric pairs over 6-day interval (Yagüe-Martínez et al., 2016). All the used acquisitions are from 3 ascending geometries, defined by the relative orbit number (RON): RON 58 (29 images), RON 160 (31 images) and RON 87 (30 images). In total, 90 acquisitions and 85 InSAR pairs from May 3–October 31, 2018 are used covering the vegetation period (after the snowmelt in April to October) including the full peat extraction season in Estonia. Acquisitions for July 26 and August 19 (RON 58) are missing. The acquisition time for all the three RONs is around 4 pm UTC which corresponds to 7 pm in local summer time (EEST). The sunset is at 9 pm in the beginning of May, later than 9 pm till mid-August and before 7 pm since the end of September (which means before a SAR acquisition in October).

2.5. SAR processing

The main processing of Sentinel-1 data was done with the processing chain developed by Kappazeta Ltd. (Tamm et al., 2016; Kappazeta, 2019). All together 90 acquisitions from 3 ascending geometries (RONs 58, 160 and 87) over May 3–October 31 were processed resulting in 85 InSAR pairs. The processing chain utilises the SNAP Toolbox (ESA, 2019). Backscatter coefficient σ^0 in VV and VH polarisations and VV/VH ratio are output for individual images and signal-to-noise ratio (SNR) corrected InSAR coherence magnitude $|\gamma|$ for 6-day image pairs.

σ^0 and $|\gamma|$ are calculated based on the Sentinel-1 Product Definition (Bourbigot et al., 2016). The processing chain includes the SNAP operators: Applying Orbit File, Thermal Noise Removal, Calibration and Range-Doppler Terrain Correction. The InSAR processing chain includes: S1 TOPS Coregistration with ESD, Coherence estimation (with flat-earth and topographic phase removal), TOPS Deburst, Range-Doppler Terrain Correction and SNR correction. SRTM 1 s and bilinear interpolation was used in coregistration and terrain correction; the shifting window size for coherence estimation was 5 in azimuth and 19 in range (5x19 pixels). A coherence estimation window size approximating 70x70 m is chosen to best address the trade-off between estimation bias towards higher coherence values and loss of spatial resolution (Touzi et al., 1999; Dahdal, 2011; Tamm et al., 2016).

The mean, median, maximum, minimum and standard deviation (SD) of σ^0, VV/VH ratio and $|\gamma|$ are calculated for each single predefined polygon. The characteristics are calculated from the ground projected SAR pixels inside any given individual inner buffered polygon for a given date (σ^0) or an image pair ($|\gamma|$). The polygons are buffered inside (31 m) to exclude the pixels affected by neighbouring production areas, stockpiling and roads and to compensate the absolute geolocation error of Sentinel-1 products (Bourbigot et al., 2016; Schubert et al., 2017). That is how the mean or SD of σ^0 and $|\gamma|$ should be understood in every figure of this paper. The only exception is Table 1 where VV median coherence of the polygons are aggregated into classes and the table presents figures calculated inside a class.

In total, 46 polygons are included in this study. Amongst them, 18 are production blocks (defined by the producer), 10 abandoned areas and 18 from the open bog. The polygons of open bog and abandoned cutover peatland, which serve as reference for undisturbed conditions, are based on the classification provided in the Estonian Topographic Database (Estonian Land Board, 2019). Images from RON 160 cover all 46 polygons, images from RON 58 cover 39 and RON 87 covers 19 polygons (the approximate location of tracks relative to polygons is given in Fig. 1a).

We compiled a multi-temporal dataset containing the characteristics calculated for each polygon for every given date, the peat producer reported extraction status data and the precipitation estimates. Subsequent statistical analysis of the dataset was performed in R software with the Mann–Whitney U test (pairwise.wilcox.test function in R), known also as the Wilcoxon rank-sum test (Mann and Whitney, 1947; Hart, 2001; McDonald, 2014) following the Benjamini–Hochberg (BH) procedure (Benjamini and Hochberg, 1995). We chose a nonparametric test as our data is not normally distributed, and in addition our sample size is relatively small.

We do not distinguish the extraction sites (Soosaare, Tässi and Sangla). All the polygons are included indiscriminately in all the calculations with the aim of having a sufficient sample size (of extraction blocks and reference areas) for the statistical analysis. Only to study the influence of different works constituting the milled peat harvest cycle on coherence the Sangla site is analysed separately. The data from Sangla cover the full harvest cycle (milling, turning, harvesting) while Soosaare and Tässi datasets contain only harvesting events.

An additional stack of coherence images from RON 160 over the period of April 22–October 31, 2018 (32 images) was produced for visualisation purposes only, using SNAP Desktop (version 7.0.0). The Python module Snappy provided by SNAP was used to automate processing (Peters, 2016). The guidelines for Sentinel-1 TOPS DInSAR processing (Braun and Veci, 2020; Yagüe-Martínez et al., 2016; Fielding, 2018) were followed for coherence estimation. To ensure the comparability, the processing chain and parameters are identical to what Kappazeta Ltd. applied except for SNR which was not included.

2.6. Change detection based on coherence

Interferometric coherence (Zebker and Villasenor, 1992) is a normalised measure of similarity between two SAR acquisitions, quantifying changes in amplitude and phase of the image pixels in a complex cross correlated InSAR image pair (Preiss et al., 2006; Scott et al., 2017). Coherence is high when the position and physical properties of the scatterers within the averaging window are similar for both images. Coherence decreases with change in position and physical properties of the scatterers between acquisitions (Tamm et al., 2016; Scott et al., 2017). Undisturbed non-vegetated bare grounds display good InSAR coherence until surface altering events happen (Wegmüller and Werner, 1995; Schepanski et al., 2012). In analogy, in peat extraction sites coherence between two SAR acquisitions is expected to remain high until extraction or other surface altering work has taken place to lower coherence.

3. Results

3.1. Detection of active peat extraction sites

In Fig. 2, a summary of seasonal coherence for different land cover classes is shown. Median coherence of the polygons (displayed in Fig. 1a) on different acquisition dates and from different RONs during the main harvest season (till August 3) are assembled by land cover (extraction site, abandoned cutover peatland, open bog). In the figure, a box shows the interquartile range (IQR) of the 25–75 percentile (covering central 50% of the data). Whiskers indicate the range of a set of data (if no more than 1.5 times the IQR from the box (R Documentation, 2019)), beyond whiskers the outliers are displayed. A notch surrounding a median shows the confidence interval. If the notches of two plots do not overlap there is evidence of 95% confidence that their medians differ, although it should not be regarded as a formal test (Chambers et al., 1983; R Documentation, 2019). During the main peat extraction season, the median InSAR coherence magnitude $|\gamma|$ of the production blocks in both polarisations (0.186 in VV and 0.171 in VH) is significantly lower (by Mann–Whitney U test $p < 0.001$) from both the open bog (0.601 in VV; 0.379 in VH) and abandoned cutover peatlands (0.579 in VV; 0.394 in VH). Though variability in the extraction site group is higher in VV, also the distance between its IQR and the IQR of open bog and abandoned area is bigger in VV. Therefore, VV is preferred in the following analyses. The open bog and cutover are inseparable from each other ($p > 0.05$) in either polarisation (Fig. 2). Thus, both are usable as reference area standing for what an undisturbed extraction area could look like.

Beyond the main season when only occasional maintenance works are carried out such a distinction of the extraction area does not occur. Instead, the production area (VV median $|\gamma|$ 0.666) does not differ from the abandoned area ($|\gamma|$ 0.710) in either polarisation during August–October (the post-main season). The open bog differs from the both ($|\gamma|$ 0.625, $p < 0.001$) with its smallest variability and lowest median. The variability among the extraction blocks is the highest due to the occasional ongoing maintenance works. The earthworks become improbable when the temperature falls, evaporation is low and the peat too wet to support heavy machinery in October. In October, all the 3 groups differ ($p < 0.001$) and the extraction area displays the highest coherence and smallest variability (extraction area VV median $|\gamma|$ 0.868, abandoned area 0.803, open bog 0.703). VH polarisation behaves similarly, just with lower $|\gamma|$ values and greater variability in the active and abandoned extraction area. The visual interpretation of the additionally created InSAR image stack of RON 160 (which contrary to the main processing chain spans also to the preseason; no characteristics calculated for the polygons, visualisation purposes only) reveals high

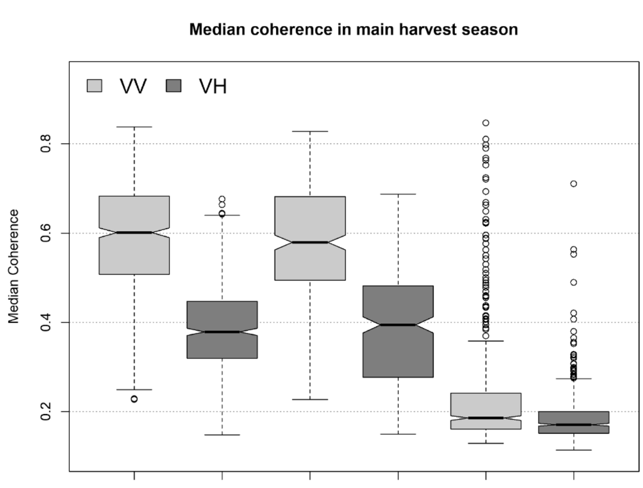

Fig. 2. Median coherence of polygons (median $|\gamma|$ of the individual ground projected SAR pixels in a given polygon in a given image pair) from different land cover classes at any given 6-day acquisition period during the main peat extraction season in both VV and VH polarisations. The extraction area significantly differs from the open bog and abandoned peatland ($p < 0.001$).

coherence in April 22–28 and April 28–May 4 for all the production blocks in Soosaare, Tässi and Sangla. Similarly, the abandoned sites and the open bog are also characterised by the coherence comparable to October (Fig. 3a).

In Fig. 4, the summary of seasonal behaviour of backscattering coefficient σ^0 is presented for VH and VV polarisation for three land use classes. As shown in Fig. 4a, σ^0 also responds to peat harvesting, but the response is less distinct than for coherence. Contrary to coherence, the faculty of discrimination in σ^0 is more distinct in VH where all groups differ significantly from each other ($p < 0.001$) (Fig. 4a). Herein, the extraction sites and unmanaged open bog differentiate the most. However, the VH signal is ~10 times weaker than VV. In October (Fig. 4b) when the soil water content is higher and peat extraction related works are improbable, the unmanaged open bog is significantly different from the other classes ($p < 0.001$). Here VV is more sensitive than VH. The difference between the extraction and cutover area ($p < 0.05$) indicates also that differentiation of these classes could be feasible (Fig. 4b).

3.2. *Evaluation of peat extraction intensity*

The polygons of production blocks are divided into intensity classes according to how many times the harvesting cycle was repeated there during the main harvest season. Group "6–10 cycles" consists of 3 blocks, "11–15 cycles" – 8 and "16 cycles" – 7 blocks. Polygons from the open bog and abandoned peatland serve as reference for undisturbed conditions. Each data point corresponds to the median coherence of a 6-day acquisition period from the corresponding polygon. The peat extraction intensity classes display similar medians and are statistically inseparable, both in VV and VH. Also the open bog and abandoned area are similar to each other (Fig. 5). Though, the increasing variability of coherence coinciding with decreasing number of harvesting cycles could possibly give means for assessment of extraction intensity via mean, standard deviation (SD) and interquartile range (IQR) which display clear differences in VV (Table 1). In VH, variability among the extraction intensity classes is minimal.

3.3. *Detection of peat extraction events*

As shown (Fig. 2), the seasonal median coherence in both polarisations is suitable to differentiate area of active peat extraction from abandoned or unmanaged peatlands. However, as VV is more sensitive the further analysis focuses on VV. Fig. 6 illustrates changes in coherence in the production block Sangla 1. Coherence is significantly lower during the season of peat harvesting compared to the image pair July 27–August 2 which marks the known end of regular harvesting (see also Fig. 3b,c). Coherence is stable and highest in October when probability for earthworks is reduced as temperatures fall, evaporation is lowest and peat becomes wet. After the peat production season (no in situ data available), coherence behaviour is erratic and leaves it unanswered whether it is caused by surface altering works (e.g. profiling), precipitation or soil moisture. Therefore, comparison with a reference polygon from a known undisturbed site or combining multiple RONs is introduced for further analysis.

As shown in Fig. 6 and Fig. 3, coherence in an extraction site when works are carried out is significantly lower compared to the reference areas of abandoned site and open bog. Similarly, in image pairs August 20–26 and September 13–19 only the extraction site displays low coherence. Thus, that has to correspond to activities. Contrary, in August 14–20 all 3 polygons display strong decorrelation due to heavy rain on August 20 (18 mm/d). The decorrelation caused by the rainfall may have obscured the effect of possible preceding earth works. Though, rain on August 20 does not destroy coherence in August 20–26 as both days were rainy (18 and 2.3 mm/d, respectively) and soil is expected to be wet in both acquisitions. However, the high 3-day precipitation sum on preceding August 14 (8.8 mm) did not help to maintain coherence in

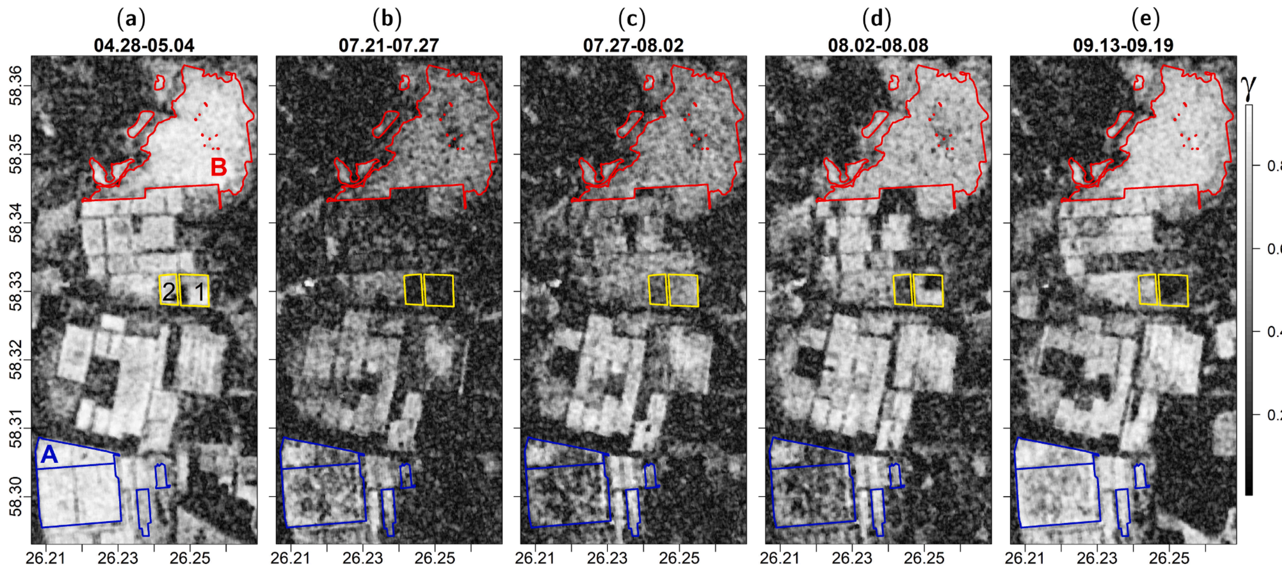

Fig. 3. VV median coherence $|\gamma|$ for polygons in the Sangla site for RON 160 in April 28–May 4 (a), July 21–27 (b), July 27–August 2 (c), August 2–8 (d) and September 13–19 (e). Production blocks Sangla 1 and Sangla 2 (black ID numbers; image a) are marked with yellow contour. The open bog (B) is red. Abandoned blocks are blue, polygon A is marked (a). (For interpretation of the references to colour in this figure legend, the reader is referred to the web version of this article.)

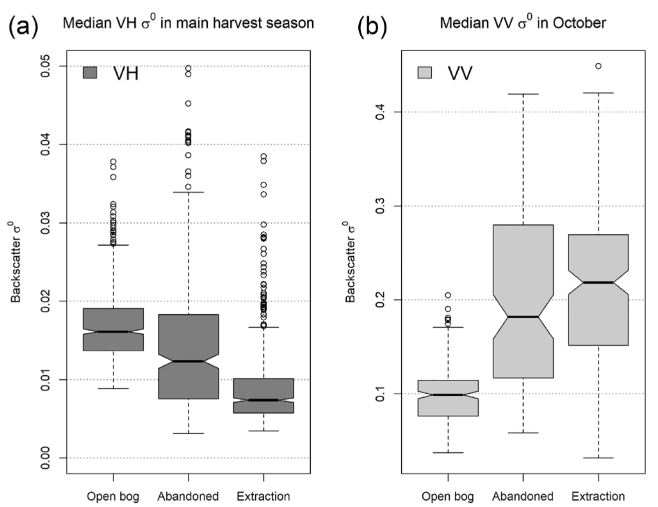

Fig. 4. Median backscatter coefficient σ^0 of polygons from different land cover classes on any given 6-day acquisition period during the main peat extraction season (a) and in October (b) when peat extraction related works are improbable, in VH and VV polarisation respectively (shown is the polarisation where the distinction manifests stronger). All the groups differ significantly ($p < 0.001$) during the main harvest season (a). In October (b) the open bog is significantly different from the rest ($p < 0.001$); the extraction and abandoned area also differ ($p < 0.05$).

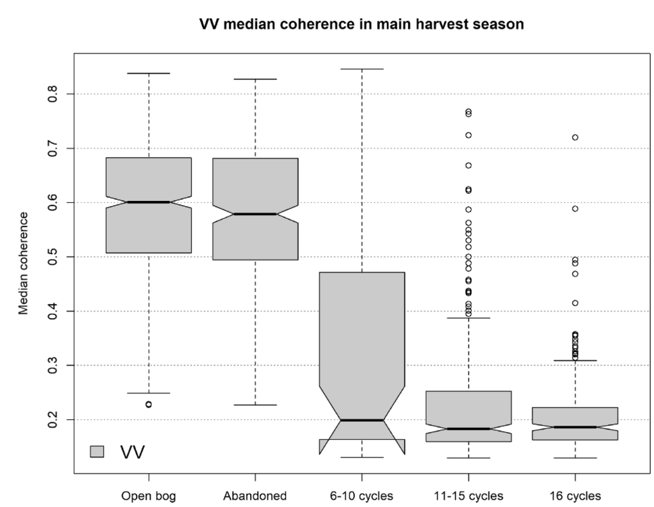

Fig. 5. VV median coherence at any given 6-day acquisition period grouped to extraction frequency classes according to how many times the harvesting cycle was repeated in the corresponding polygon during the main harvest season. The harvest intensity groups have similar median values and are statistically indistinguishable ($p > 0.05$), though they display different internal variability.

August 14–20. Therefore, in further analysis we use 1-day precipitation as it correlates better with the coherence. The peat extraction sites are effectively drained by the dense network of ditches and the water table lies low below the surface. The nearly constant water table in the site throughout the years of peat extraction is achieved by extraction field profiling, and the annual regular maintenance and deepening of ditches according to the lowering of the surface of the extraction fields. In the summer months when the temperature and evaporation is high, the upper peat layer dries and becomes hydrophobic. Therefore, the rainwater evaporates or drains quickly to the ditches without filling pores in the peat. Nevertheless, there is always some moisture in the peat and that is why turning and drying of the peat after the milling is necessary (for harvesting, the peat humidity has to be lowered to ~40% (Cleary

Table 1
Figures describing the internal variability inside the extraction classes grouped by the extraction frequency in a polygon. VV median coherence of individual polygons at any given 6-day acquisition period during the main extraction season are aggregated into classes. "Class" indicates the number of harvest cycles repeated; "Count" stands for the number of observations from the corresponding polygons; standard deviation is "SD"; and interquartile range – "IQR".

Class	Count	Median	Mean	SD	IQR
16 cycles	225	0.186	0.207	0.0753	0.0595
11–15 cycles	285	0.183	0.228	0.115	0.093
6–10 cycles	60	0.199	0.318	0.225	0.302
Abandoned	328	0.579	0.577	0.134	0.187
Open bog	646	0.601	0.594	0.116	0.175

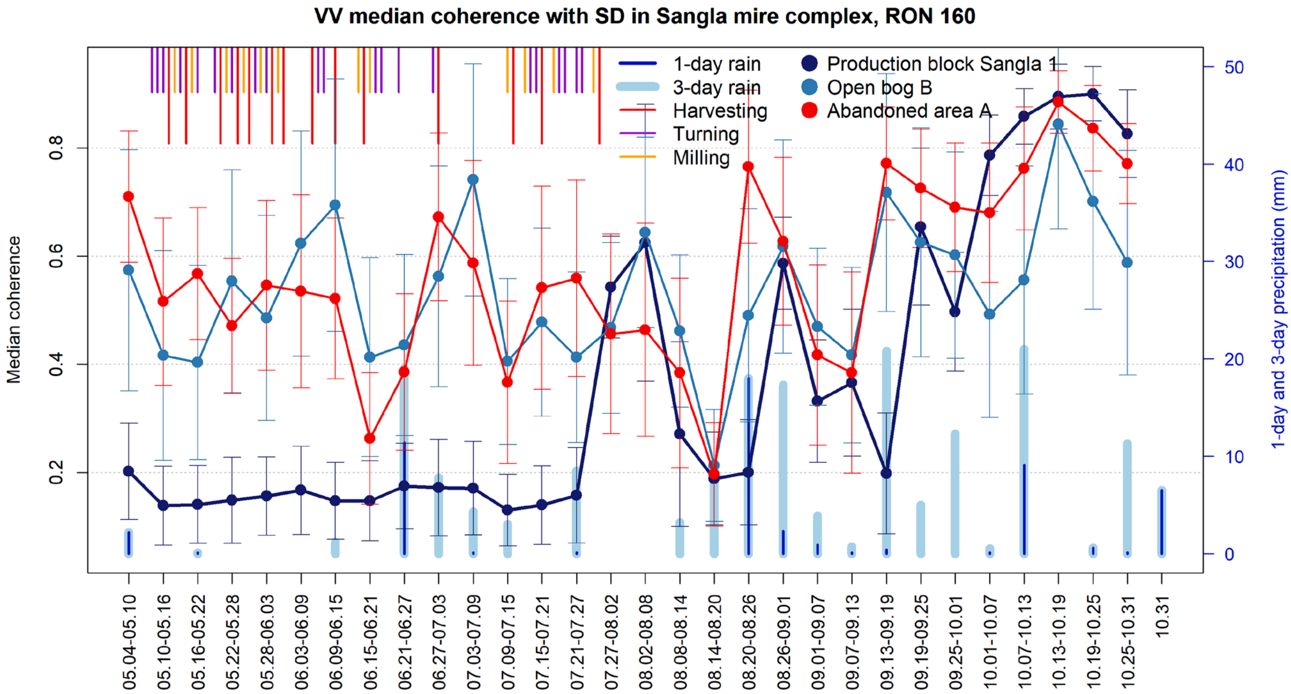

Fig. 6. Coherence median values with standard deviation of Sangla extraction block 1, abandoned area A and open bog B from RON 160 (for location of A, B and bloc 1 see Fig. 3b). 1-day and 3-day precipitation sum and the recorded works constituting the peat harvest cycle are shown.

et al., 2005; Eesti Turbaliit, 2019)). Also, the increased peat decomposition rate in the deeper extraction layers alters the hydraulic properties of the peat (pore size, water conductivity, water field capacity etc.). That affects the length of the period when milling, turning and peat harvesting can be performed but has only a minor effect on the water table depth.

As peat production permanently alters the peat surface, the sequence of image pairs from different RONs with an offset of a few days have all to reveal the same loss of coherence. In our study we could compare up to 3 RONs depending on the availability of SAR acquisitions. If only one image (or two images) of the sequence shows loss in coherence, the loss can be attributed to something temporal (like the rain in one of either acquisitions) which affects that particular image pair but leaves the pairs from other RONs intact as they overlay that particular date but do not begin or end with it. As shown in Fig. 7, coherence seems to be almost insensitive to incidence angles. The time series of RON 87 in near range

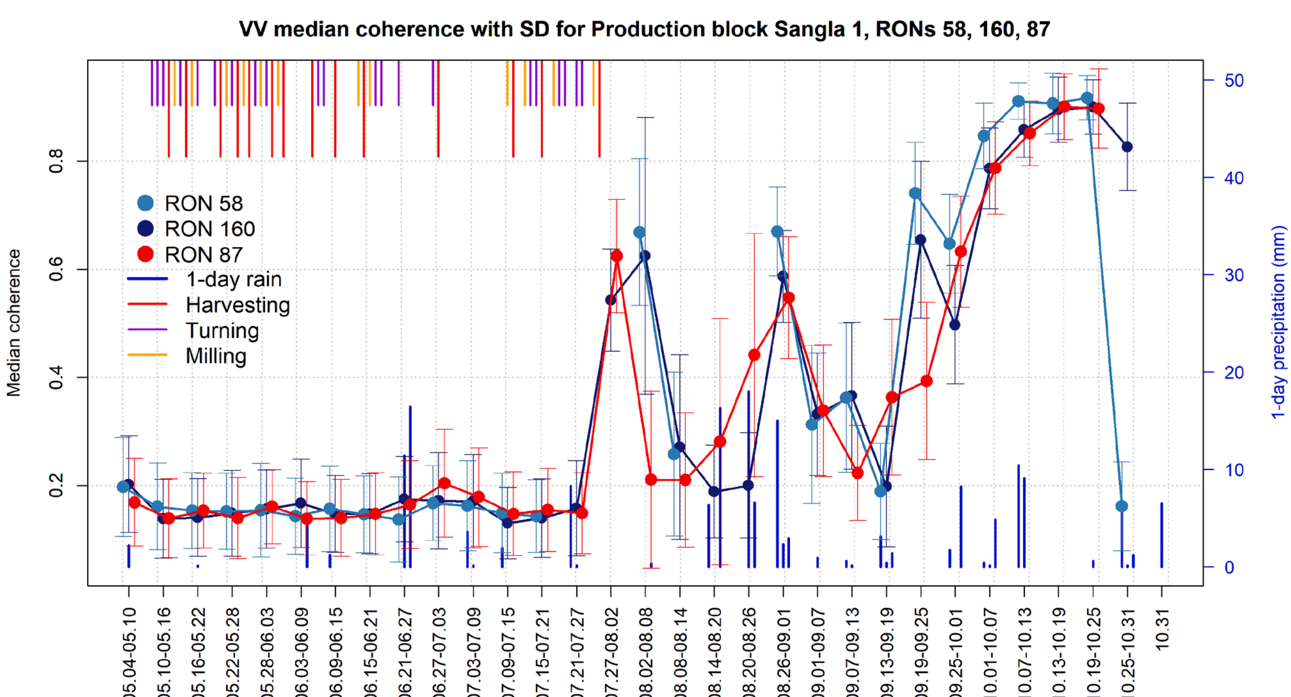

Fig. 7. VV coherence median with standard deviation of Sangla production block 1 from 3 RONs. The right axis shows 1-day and 3-day sum of precipitation. The top shows recorded peat extraction related works.

(incidence angle ~30°) and RON 58 far range (~45°) show little to no difference. All 3 RONs agree and record peat extraction during the main harvest period (ended on July 25). Accordingly, all the three RONs with low coherence around September 13–19 (see Fig. 3e) reveal some work done out of the main season. Also, the cluster of low values at August 8–14 probably reveals activities. In August 20–26 RON 160 shows a work. The relatively low value of RON 87 in August 15–21 may accord with that, though we do not have the acquisition from RON 58 for confirmation. Contrary, the October 24–30 low value (RON 58) cannot be caused by works as the other 2 RONs show good coherence. Hence, the decorrelation has to be due to weather conditions. October 24 witnessed 5.9 mm/d of rain and average air temperature of 3.2° C while October 29 had 0.0 mm/d and 0.1° C which may indicate the possibility for frost.

3.4. Detection of partially harvested areas

Peat extraction blocks are relatively large. The smallest block of our study (Tässi 6) covers 8.3 ha (300x275 m), the largest (Tässi 1) 25.3 (315x800 m). The ground projected terrain corrected resolution of a Sentinel-1 image approximates 20x20 m; the coherence estimation window we used approximates 70x70 m. Thus, the production blocks are large enough to distinguish also between the areas inside a block. Such distinguishing may be useful if some extraction fields (about 20x300 m) forming a block have not been harvested for some reason. Detection of partially harvested areas is not achievable by using coherence median only. SD alone cannot distinguish between fully harvested and non-harvested areas as both display low variability in coherence values inside a block. Though, combining the median and SD of coherence pixel values in a polygon (production block) makes distinction between fully and partly harvested areas and areas with no activity possible as seen in Fig. 8 from July 21–27 and illustrated by Fig. 9 (displaying all of the 3 case study areas) and Fig. 3b (fully harvested). The characteristics calculated for the polygons, the visually interpreted coherence images from RON 160 and the in situ data of the harvesting events from Sangla, Soosaare and Tässi (the latter two containing the measure of area harvested) agree with each other. SD of VV $|\gamma|$ is ~0.2 for the partially harvested blocks and ~0.1 for the full and no harvest (Fig. 8). VH is less sensitive to partial extraction. In July 21—27, VH SD values for partial harvest are ~0.13, whereas harvested and unharvested blocks display less than 0.11. Contrary, σ^0 SD is unable to discriminate partial extraction.

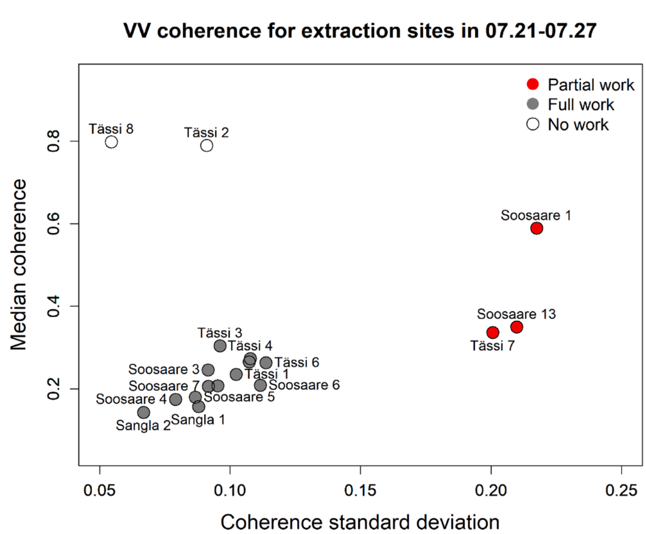

Fig. 8. Production blocks in July 21–27 for RON 160. Left axis shows the VV median coherence of a polygon and the coherence standard deviation is on bottom axis. Gray marks full harvest, red partial harvested and white no activity. The Sangla, Soosaare and Tässi datasets of harvesting events agree with the SAR results. (For interpretation of the references to colour in this figure legend, the reader is referred to the web version of this article.)

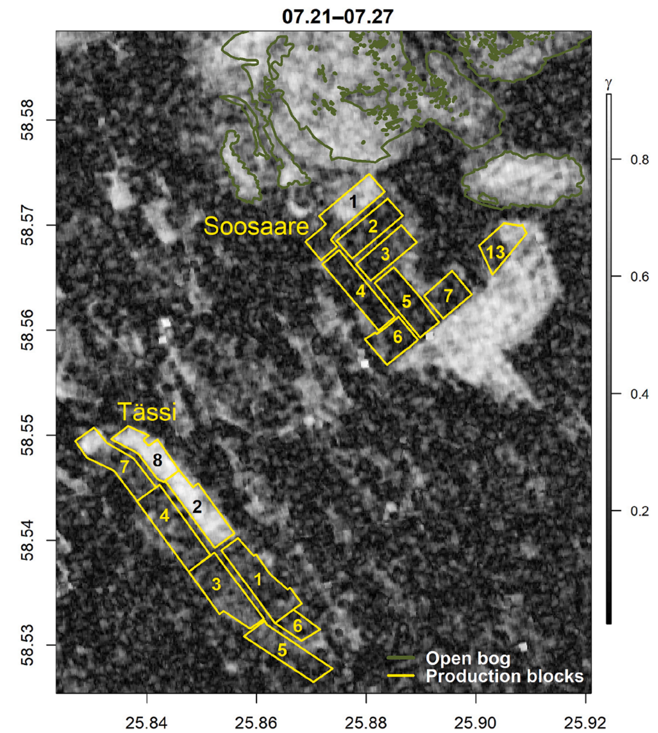

Fig. 9. Soosaare and Tässi extraction sites in July 21–27, Sentinel-1 RON 160. Soosaare and Tässi datasets of harvesting events agree with SAR results.

However, interpretation is complicated by lacking in situ data for the off season. For Soosaare block 13 the main season had ended but activity was detected by SAR. Hence, it is expected to be some maintenance work but we lack verification. Additionally, Fig. 6 and Fig. 3d depict partial extraction in Sangla block 1 in August 2–8, although no in situ data are available.

3.5. Effects of precipitation

Rain does not seem to influence neither median coherence nor coherence SD notably as demonstrated in Section 3.3 (Figs. 6, 7). It seems the heavy rain on one acquisition date may reduce the coherence to noise level only if the other date experiences dry conditions.

Contrary, σ^0 responds to the rainfall in all the land cover classes (Fig. 10). Both polarisations show similar patterns while VV σ^0 is approximately 10 times stronger than VH though. σ^0 seems to be sensitive to 1-day precipitation but insensitive to 3-day precipitation, which indicates that the soil dries off in one day. The declining trend of the σ^0 in May, recognisable in all the three polygons of different land cover (Fig. 10), is assumed to be related to the decrease in surface humidity. The maximum water table is reached in the spring after the snowmelt (April). Thereafter, the water table lowers rapidly in May, which is associated to drying of the upper layers of the peat.

However, σ^0 depends on the incidence angle and incidence angles are different for polygons far away in SAR range within the same RON and different also for the same polygon between RONs. Thus, polygons are not directly comparable and quantitative analysis is complicated. Fig. 11 shows how response of VV σ^0 to 1-day summarised precipitation in peat production blocks during the whole season differs by the RON. The groups of "no rain", "up to 5 mm" and "more than 5 mm" of summarised rainfall per day differ significantly from each other ($p < 0.001$) for RON 160 and 58. For RON 87, only groups "0" and "0–5" differ significantly ($p < 0.05$) and difference of "0" and ">5" is approaching to

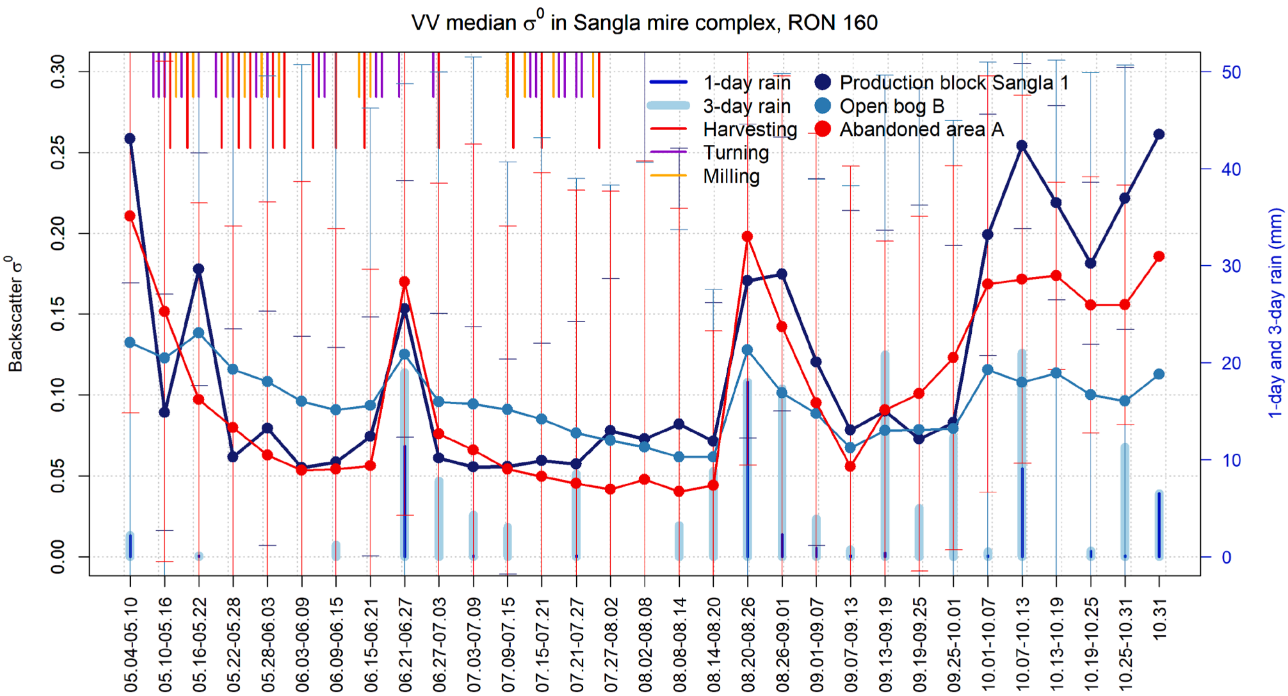

Fig. 10. VV σ^0 median values with standard deviation of Sangla extraction block 1, abandoned area A and open bog B from RON 160. The right axis shows 1-day and 3-day sum of precipitation. The top shows recorded peat extraction related works.

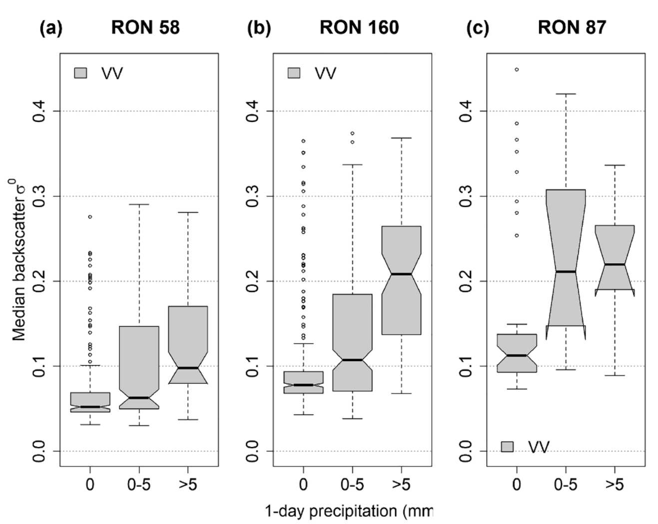

Fig. 11. VV σ^0 median in peat production blocks during the whole season by RON: 58 (a), 160 (b), 87 (c). The 1-day summarised rainfall has been grouped as "no rain" (0), "up to 5 mm" (0–5) and "more than 5 mm" (>5). Distinction between rainfall groups are most pronounced for RON 160 where each group differs from the others significantly ($p < 0.001$). For RON 87, only "0" and "0–5" differ ($p < 0.05$).

statistical significance ($p = 0.075$ and $p = 0.05$ in VV and VH, respectively). Sensitivity to rain for different RONs is slightly different in the two polarisations.

On the other hand, as seen in Fig. 10, σ^0 is not directly sensitive to surface altering works. The harvest season ended in Sangla on July 25. While coherence from all 3 RONs confirm that no work were done in the following period of July 27–August 2 (Fig. 7), σ^0 is not affected.

4. Discussion

In this study, out of the characteristics computed from SAR data we found coherence median and SD, and σ^0 median the most useful in regard to peat extraction monitoring. For minimum and maximum values and σ^0 VV/VH ratio we did not find useful outcomes. We considered herein only the shortest available temporal baseline to capture the often occurring extraction related events as accurately as possible. Contrary to the abrupt changes investigated in this paper, our previous research has shown that the peat surface remains coherent over a prolonged period of time in natural open bogs (Tampuu et al., 2020). The similar nature of $|\gamma|$ in the spring and late autumn (both periods characterised by the high peat humidity) demonstrated by the visual interpretation aligns also with what is previous known about the long term $|\gamma|$ in the open bogs (Tampuu et al., 2020).

We found InSAR coherence to be more sensitive to peat extraction related changes than σ^0. Additionally, σ^0 is dependent on the incidence angle (Adams et al., 2013; Mladenova et al., 2013) which complicates interpretation and reproducibility. Previously, Muro (2019) has advocated for coherence based change detection methods in wetlands. Also Mohammadimanesh et al. (2018) investigated the use of coherence in wetland mapping and consequently call for its synergistic use with σ^0. Such fusion for scene change detection, as both statistics measure different properties, was already proposed by Preiss et al. (2006). In our study we have identified how considering σ^0 adds information about the effect of precipitation.

Also, comparison with undisturbed reference areas helps to avoid the rain induced false positives. As shown, such areas can be either the open bog or cutover sites which behave similarly in VV during the main harvest season. The open bog is superior as a reference in robustness because open bogs are easy to identify on the map and they tend to be situated in close vicinity of extraction areas. Additionally, there may be no abandoned sites around. Furthermore, the abandoned areas located in a complex with active fields may experience surface altering activities such as stockpiling, driving vehicle or maintenance of ditches. In the current study, the polygons of abandoned area were deliberately chosen so that the risk of such events was minimised (the risk could not be ruled out entirely).

In our study we used two types of open bog polygons. One type was with large areal cover which contain a significant degree of heterogeneity in vegetation and micro relief. The other are small uniformity based polygons deliberately extracted from a bigger intact open bog area. Both types of polygons acted similarly and maintained coherence. However, small open bog plots in direct contact with the extraction area tended to lose coherence, making them unsuitable as a reference area. Consequently, those plots are not included in the analysis. Loss of coherence is probably connected to bigger groundwater table fluctuations in drainage affected areas. Differences in water table depth seems to be the main factor determining long term temporal InSAR coherence in the open bog according to Tampuu et al. (2020).

We found VV coherence to be more responsive to surface altering works than VH. Also, VV σ^0 is around 10 times stronger than in VH. Though, VH signal being weaker and thus more affected by the noise should not be the reason for lower coherence values because the coherence is SNR-corrected. Cross polarisation is known to be strongly sensitive to vegetation and volumetric scattering as vegetated areas have strong backscatter while the bare surface has low. Contrary, co-polarisation backscattering is significantly influenced by the soil characteristics and by the soil moisture (Pampaloni et al., 1997; Millard, 2016; Bousbih et al., 2017).

The loss of coherence in the bare non-vegetated peatland has to be caused by a combination of two main factors in unknown proportions. These are the geometric change via physical dislocation of soil parcels of the uppermost layer and changes in soil moisture, as shown for agricultural lands (Wegmüller and Werner, 1997) and other low-biomass areas such as clear cuts (Thiel et al., 2009). In addition to the physical change of the surface, the lower peat layers which become exposed through milling, turning and harvesting contain more moisture than the dried-off topmost layer. Herein, soil moisture is important factor determining penetration depth of the radar signal (Nolan et al., 2003). Direct dependency of InSAR phase on soil moisture has been shown in agricultural lands (Barrett et al., 2013; De Zan et al., 2014; Zwieback et al., 2015) where change in soil volumetric water content can cause a change of up to 60 mm in C-band penetration depth (Nolan and Fatland, 2003). However, no quantitative research of penetration into peat is available (Millard, 2016). As drying only affects a thin surface layer of peat, the change in penetration depth is expected to be within reasonable range and should not be affected severely by extraction. That assumption is supported by our findings that the effect of rain on coherence is minor compared to the harvest related works. It seems only heavy rain on one acquisition while there are dry conditions on the other can decorrelate the scene similarly to works. That is in contrast to findings from the forest (Santoro et al., 2002) and grasslands (Tamm et al., 2016) which attribute the rainfall a great importance but in concord with results from natural open bogs (Tampuu et al., 2020), regarding rain as of modest importance.

We have shown how SAR response to the milling, turning and extraction events cannot be discriminated. Furthermore, sometimes a block is harvested partly. That may result as planned or unplanned due to unexpected weather. In the latter case, all the previous works of harvest cycle have been conducted on the full extent of the block and the consequent decorrelation reflects these works instead of the extent of the eventually harvested area. Contrary, if the partial work is planned it is detectable as all the works of the cycle are performed on the same limited portion of the block. Those assumptions are supported by the data from Soosaare and Tässi which contain the areal cover of the harvest but no notion about the extent of milling or turning. Indexing based on the reported extent of the harvested area (full vs partial areal cover of the work) did not reveal differences between groups. Additionally, the depth of harvesting varies according to whether it is horticultural or energy peat and is also dependant on soil humidity. Therefore, it is not possible to asses the harvested area simply from coherence, nor it is possible to adequately calculate the volume of extracted peat even if the areal extent is known.

However, segregating production blocks by frequency of harvesting seems promising. Previously, Muro et al. (2019) showed the benefit of deploying frequency of change in landcover classification and Muro (2019) links these findings to InSAR coherence. Thus, our preliminary findings could be developed to operational use via frequency of change based mapping (for example as proposed by Muro et al. (2019)). Being able to distinguish between active and abandoned peat extraction areas and also to discriminate dedicated areas according to the intensity of use would benefit climate mitigation by helping to call for the depletion of already opened blocks instead of opening new. Also, similar behaviour of VV σ^0 in the active and abandoned extraction areas and their distinction from the open bog might be utilised in evaluation of restoration success of cutover peatlands.

As the main aim of this study was to demonstrate the feasibility of detection of the peat extraction related activity. The next step could be developing an operational algorithm. The image pairs of 6-day temporal resolution are available from the last days of April till November which is the sensing period of Sentinel-1B IW mode over Estonia and which covers the growing season. The coverage of Sentinel-1B is similar in the rest of the Baltic Sea region, with the Sentinel-1B switching to Extra Wide Swath mode (EW) for sea-ice monitoring during the winter (2–8 months, depending on the region). The temporal resolution is constantly 6 days in the rest of Europe. The worldwide coverage is mainly with a 12-day revisit (Copernicus Space Component Mission Management Team, 2019). Visual interpretation of each individual image pair seems to be the reliable-most method, though highly time and resource consuming. A feasible alternative is the polygon based time series approach which is more reliable the more RONs cover the polygon of interest. Including both ascending and descending orbits (3 and 1 over Estonia, respectively) would make 4 SAR acquisitions available in 3 days followed by a 3 day-period of no acquisitions. That should increase the reliability (our study used only ascending orbits). Nevertheless, adding σ^0 and comparison with reference polygons is advisable for increased reliability.

5. Conclusions

The aim of this study was to evaluate the hypotheses that Sentinel-1 6-day InSAR coherence time series allow to: 1) distinguish active peat extraction sites from abandoned sites; 2) detect peat extraction associated activities and; 3) differentiate partially harvested blocks from fully harvested areas and areas with no activity. We have demonstrated that median coherence enables to detect peat production related surface altering works and therefore also differentiate active and inactive extraction areas. For this, VV polarisation is more sensitive compared to VH. The polygon based multi-RON time series approach is sufficient for the task because coherence seems to be almost insensitive to incidence angles over peatland areas.

During the main harvest season the peat extraction area shows a VV median coherence of less than 0.2 while the abandoned area and open bog which serve as a reference for undisturbed extraction area, are close to 0.6 ($p < 0.001$). Beyond the main season when only occasional maintenance works are conducted (August–October), the production area does not differ from the abandoned area and the both display VV $|\gamma|$ around 0.7. The open bog differs from the rest ($|\gamma|$ around 0.6; $p < 0.001$). The highest variability is recorded among the extraction blocks, due to the occasional ongoing maintenance works. In October when the climatological conditions make the earthworks improbable, the extraction area displays the highest coherence (close to 0.9 in VV) with smallest variability. The $|\gamma|$ of the abandoned area is 0.8 and open bog 0.7, all the 3 groups differ ($p < 0.001$). The behaviour of VH is similar, with lower $|\gamma|$ values and greater in-group variability in the active and abandoned extraction area. Though, it was not possible to discriminate harvesting from other activities or derive estimates of harvested peat volume. However, the potential for coherence based peat extraction intensity estimation is demonstrated.

Also, an indication is given how partially extracted areas could be distinguished from fully harvested and not harvested areas by the coherence standard deviation. According to the results, the influence of rainfall on the detection of peat harvesting related works is modest. Only the heavy rain on one of the acquisitions of the image pair whereas the other acquisition is from dry conditions seems to cause decorrelation comparable to surface altering works. However, deploying images from multiple consecutive orbits or including backscatter intensity σ^0 or reference polygons of undisturbed area to the analysis, help to reduce risk of rain induced false positives. For the included viewing geometries, except RON 87, σ^0 response to no rain (0 mm/d) and to precipitation (0–5 or > 5 mm/d) differs significantly ($p < 0.001$).

The novelty of our approach, beside applying it to peat extraction, is the indication of the possibility for partial work detection based on the coherence standard deviation and using σ^0 or reference polygons for the rain induced error mitigation. Our findings could enhance more efficient resource management and monitoring for climate change mitigation. Developing an operational algorithm for peat extraction identification should be undertaken in future studies. Such algorithm might be adjustable to any other type of open pit mining.

CRediT authorship contribution statement

Tauri Tampuu: Formal analysis, Methodology, Visualization, Writing - original draft. **Jaan Praks:** Methodology, Supervision, Writing - review & editing. **Ain Kull:** Conceptualization, Methodology, Writing - review & editing. **Rivo Uiboupin:** Conceptualization, Methodology, Supervision. **Tanel Tamm:** Software, Supervision. **Kaupo Voormansik:** Conceptualization, Software.

Declaration of Competing Interest

The authors declare that they have no known competing financial interests or personal relationships that could have appeared to influence the work reported in this paper.

Acknowledgement

This study is part of PhD research supported by the European Union from the European Regional Development Fund. Also, the study was financially supported by the European Regional Development Fund within "National Programme for Addressing Socio-Economic Challenges through R&D (RITA)", Estonian Research Council grant PRG352 and State Forest Management Centre grant LLTOM17250. The applied research for Sentinel-1 InSAR time series applications was supported by the project "Data Analytics for Optimizing Agricultural Monitoring" financed by the European Regional Development Fund under Grant No. EU48684. The authors would like to thank Anto Aasa (University of Tartu) for helping with R, and Datel AS (Estonia) and Juhan-Peep Ernits (Tallinn University of Technology) for providing computing capacity.

References

Adams, J.R., Rowlandson, T.L., McKeown, S.J., Berg, A.A., McNairn, H., Sweeney, S.J., 2013. Evaluating the Cloude-Pottier and Freeman-Durden scattering decompositions for distinguishing between unharvested and post-harvest agricultural fields. Can. J. Remote Sens. 39, 318–327. https://doi.org/10.5589/m13-040.

Askne, J., Dammert, P., Ulander, L., Smith, G., 1997. C-band repeat-pass interferometric SAR observations of the forest. IEEE Trans. Geosci. Remote Sens. 35, 25–35. https://doi.org/10.1109/36.551931.

Askne, J., Santoro, M., Smith, G., Fransson, J., 2003. Multitemporal repeat-pass SAR interferometry of boreal forests. IEEE Trans. Geosci. Remote Sens. 41, 1540–1550. https://doi.org/10.1109/TGRS.2003.813397.

Barrett, B., Whelan, P., Dwyer, E., 2013. Detecting changes in surface soil moisture content using differential SAR interferometry. Int. J. Remote Sens. 34, 7091–7112. https://doi.org/10.1080/01431161.2013.813654.

Benjamini, Y., Hochberg, Y., 1995. Controlling the false discovery rate: a practical and powerful approach to multiple testing. J. Roy. Stat. Soc.: Ser. B (Methodol.) 57, 289–300. https://doi.org/10.1111/j.2517-6161.1995.tb02031.x.

Beyer, C., Höper, H., 2015. Greenhouse gas exchange of rewetted bog peat extraction sites and a Sphagnum cultivation site in northwest Germany. Biogeosciences 12, 2101–2117. https://doi.org/10.5194/bg-12-2101-2015.

Bourbigot, M., Johnsen, H., Piantanida, R., Hajduch, G., 2016. Sentinel-1 Product Definition. Issue 2.7, S1-RS-MDA-52-7440. https://sentinel.esa.int/web/sentinel/user-guides/sentinel-1-sar/document-library/-/asset_publisher/1dO7RF5fJMbd/content/sentinel-1-product-definition. Accessed: 29.04.2020.

Bousbih, S., Zribi, M., Lili-Chabaane, Z., Baghdadi, N., El Hajj, M., Gao, Q., Mougenot, B., 2017. Potential of Sentinel-1 radar data for the assessment of soil and cereal cover parameters. Sensors (Basel, Switzerland) 17. https://doi.org/10.3390/s17112617.

Braun, A., Veci, L., 2020. Sentinel-1 toolbox TOPS Interferometry Tutorial. ESA. http://step.esa.int/docs/tutorials/S1TBX%20TOPSAR%20Interferometry%20with%20Sentinel-1%20Tutorial_v2.pdf. Accessed: 17.03.2020.

Chambers, J.M., Cleveland, W.S., Kleiner, B., Tukey, P.A., 1983. Graphical Methods for Data Analysis. Wadsworth & Brooks/Cole, California, US.

Chapman, S., Buttler, A., Francez, A.J., Laggoun-Défarge, F., Vasander, H., Schloter, M., Combe, J., Grosvernier, P., Harms, H., Epron, D., Gilbert, D., Mitchell, E., 2003. Exploitation of Northern Peatlands and biodiversity maintenance: a conflict between economy and ecology. Front. Ecol. Environ. 1, 525–532. https://doi.org/10.2307/3868163.

Cleary, J., Roulet, N.T., Moore, T.R., 2005. Greenhouse gas emissions from canadian peat extraction, 1990–2000: A life-cycle analysis. AMBIO: A J. Hum. Environ. 34, 456–461. doi:10.1579/0044-7447-34.6.456.

Copernicus Space Component Mission Management Team, 2019. Sentinel High Level Operations Plan (HLOP). Issue 3.0, COPE-S1OP-EOPG-PL-15-0020. https://sentinels.copernicus.eu/documents/247904/685154/Sentinel_High_Level_Operations_Plan. Accessed: 16.06.2020.

Dahdal, B., 2011. The use of interferometric spaceborne radar and GIS to measure ground subsidence in peat soils in Indonesia. Phd thesis. University of Leicester, Leicester, UK. http://hdl.handle.net/2381/10254.

De Zan, F., Parizzi, A., Prats-Iraola, P., López-Dekker, P., 2014. A SAR interferometric model for soil moisture. IEEE Trans. Geosci. Remote Sens. 52, 418–425. https://doi.org/10.1109/TGRS.2013.2241069.

Drösler, M., Freibauer, A., Christensen, T.R., Friborg, T., 2008. Observations and status of Peatland greenhouse gas emissions in Europe. In: Dolman, A.J., Valentini, R., Freibauer, A. (Eds.), The Continental-Scale Greenhouse Gas Balance of Europe. Springer, New York, NY. Ecological Studies, pp. 243–261. https://doi.org/10.1007/978-0-387-76570-9_12.

Eesti Turbaliit, 2019. Kaevandamine. http://www.turbaliit.ee/kaevandamine/. Accessed: 15.11.2019.

ESA, 2019. Sentinel Application Platform SNAP. European Space Agency (ESA). http://step.esa.int/main/toolboxes/snap/. Accessed: 26.05.2019.

Estonian Environment Agency, 2020. Estonian weather service, observation data, daily data. http://www.ilmateenistus.ee/ilm/ilmavaatlused/vaatlusandmed/oopaevaandmed/?lang=en. Accessed: 26.05.2020.

Estonian Land Board, 2019. Estonian Topographic Database. Geoportal. https://geoportaal.maaamet.ee/index.php?lang_id=2&page_id=618. Changed: 19.11.2019.

Fielding, E.J., 2018. SAR Interferometry for Earthquake Studies. NASA. https://arset.gsfc.nasa.gov/sites/default/files/disasters/Adv-SAR/SAR-session4.pdf. Accessed: 26.05.2019.

Gorham, E., 1991. Northern Peatlands: role in the carbon cycle and probable responses to climatic warming. Ecol. Appl. 1, 182–195. https://doi.org/10.2307/1941811.

Graf, M., Bérubé, V., Rochefort, L., 2012. Restoration of peatlands after peat extraction: Impacts, restoration goals, and techniques. In: Vitt, D., Bhatti, J. (Eds.), Restoration and reclamation of boreal ecosystems: Attaining sustainable development. Cambridge University Press, Cambridge, UK, pp. 259–280.

Hart, A., 2001. Mann-Whitney test is not just a test of medians: differences in spread can be important. BMJ 323, 391–393. https://doi.org/10.1136/bmj.323.7309.391.

Kappazeta, 2019. Replacing on-the-spot-checks on grasslands with automated mowing detection. http://kappazeta.ee/en. Accessed: 15.11.2019.

Köchy, M., Hiederer, R., Freibauer, A., 2015. Global distribution of soil organic carbon – Part 1: Masses and frequency distributions of SOC stocks for the tropics, permafrost regions, wetlands, and the world. Soil 1, 351–365. https://doi.org/10.5194/soil-1-351-2015.

Leifeld, J., Menichetti, L., 2018. The underappreciated potential of peatlands in global climate change mitigation strategies. Nature Commun. 9, 1–7. https://doi.org/10.1038/s41467-018-03406-6.

Mann, H.B., Whitney, D.R., 1947. On a test of whether one of two random variables is stochastically larger than the other. Ann. Math. Stat. 18, 50–60. https://doi.org/10.1214/aoms/1177730491.

McDonald, J.H., 2014. Handbook of biological statistics. 3 ed., Sparky House Publishing, Baltimore, US. http://www.biostathandbook.com/kruskalwallis.html. accessed: 19.11.2019.

Millard, K., 2016. Development of methods to map and monitor peatland ecosystems and hydrologic conditions using Radarsat-2 Synthetic Aperture Radar. Phd thesis. Carleton University, Ottawa, Canada. https://doi.org/10.22215/etd/2016-11581.

Mladenova, I.E., Jackson, T.J., Bindlish, R., Hensley, S., 2013. Incidence angle normalization of radar backscatter data. IEEE Trans. Geosci. Remote Sens. 51, 1791–1804. https://doi.org/10.1109/TGRS.2012.2205264.

Mohammadimanesh, F., Salehi, B., Mahdianpari, M., Brisco, B., Motagh, M., 2018. Multi-temporal, multi-frequency, and multi-polarization coherence and SAR backscatter analysis of wetlands. ISPRS J. Photogramm. Remote Sens. 142, 78–93. https://doi.org/10.1016/j.isprsjprs.2018.05.009.

Muro, J., 2019. Mapping intra- and inter-annual dynamics in wetlands. Phd thesis. Rheinischen Friedrich-Wilhelms-Universität Bonn, Bonn, Germany.
Muro, J., Strauch, A., Fitoka, E., Tompoulidou, M., Thonfeld, F., 2019. Mapping wetland dynamics with SAR-based change detection in the cloud. IEEE Geosci. Remote Sens. Lett. 16, 1536–1539. https://doi.org/10.1109/LGRS.2019.2903596.
Mustamo, P., Maljanen, M., Hyvärinen, M., Ronkanen, A.K., Kløve, B., 2016. Respiration and emissions of methane and nitrous oxide from a boreal peatland complex comprising different land-use types. Boreal Environ. Res. 21, 405–426. https://helda.helsinki.fi/bitstream/handle/10138/225772/ber21-5-6-405.pdf?sequence=1.
Nolan, M., Fatland, D., 2003. Penetration depth as a DInSAR observable and proxy for soil moisture. IEEE Trans. Geosci. Remote Sens. 41, 532–537. https://doi.org/10.1109/TGRS.2003.809931.
Nolan, M., Fatland, D.R., Hinzman, L., 2003. DInSAR measurement of soil moisture. IEEE Trans. Geosci. Remote Sens. 41, 2802–2813. https://doi.org/10.1109/TGRS.2003.817211.
Ojanen, P., Minkkinen, K., Alm, J., Penttilä, T., 2010. Soil–atmosphere CO2, CH4 and N2O fluxes in boreal forestry-drained peatlands. For. Ecol. Manage. 260, 411–421. https://doi.org/10.1016/j.foreco.2010.04.036.
Pakere, I., Blumberga, D., 2017. Energy efficiency indicators in peat extraction industry – a case study. Energy Procedia 113, 143–150. https://doi.org/10.1016/j.egypro.2017.04.042.
Pampaloni, P., Paloscia, S., Macelloni, G., Sigismondi, S., 1997. The potential of C- and L-band SAR in assessing vegetation biomass: ERS-1 & JERS-1 experiments. In: Third ERS Symposium on Space at the service of our Environment, European Space Agency, Florence, Italy, 14–21 March 1997. pp. 1729–1733. https://earth.esa.int/workshops/ers97/papers/pampaloni1/index-2.html.
Parish, F., Sirin, A., Charman, D., Joosten, H., Minayeva, T., Silvius, M., Stringer, L. (Eds.), 2008. Assessment on Peatlands, Biodiversity and Climate Change: Main Report. Global Environment Centre, Kuala Lumpur and Wetlands International, Wageningen, The Netherlands. http://www.imcg.net/media/download_gallery/books/assessment_peatland.pdf. accessed: 19.11.2019.
Peters, M., 2016. How to use the SNAP API from Python. https://senbox.atlassian.net/wiki/spaces/SNAP/pages/19300362/How+to+use+the+SNAP+API+from+Python. Changed: 19.12.2016.
Preiss, M., Gray, D., Stacy, N., 2006. Detecting scene changes using synthetic aperture Radar interferometry. IEEE Trans. Geosci. Remote Sens. 44, 2041–2054. https://doi.org/10.1109/TGRS.2006.872910.
R Documentation, 2019. Box plots. https://www.rdocumentation.org/packages/graphics/versions/3.6.1/topics/boxplot. Accessed: 01.04.2010.
Salm, J.O., Maddison, M., Tammik, S., Soosaar, K., Truu, J., Mander, Ü., 2012. Emissions of CO_2, CH_4 and N_2O from undisturbed, drained and mined peatlands in Estonia. Hydrobiologia 692, 41–55. https://doi.org/10.1007/s10750-011-0934-7.
Santoro, M., Askne, J., Smith, G., Fransson, J.E.S., 2002. Stem volume retrieval in boreal forests from ERS-1/2 interferometry. Remote Sens. Environ. 81, 19–35. https://doi.org/10.1016/S0034-4257(01)00329-7.
Schepanski, K., Wright, T.J., Knippertz, P., 2012. Evidence for flash floods over deserts from loss of coherence in InSAR imagery. J. Geophys. Res. 117 https://doi.org/10.1029/2012JD017580.
Schubert, A., Miranda, N., Geudtner, D., Small, D., 2017. Sentinel-1A/B combined product geolocation accuracy. Remote Sens. 9, 607. https://doi.org/10.3390/rs9060607.
Scott, C.P., Lohman, R.B., Jordan, T.E., 2017. InSAR constraints on soil moisture evolution after the March 2015 extreme precipitation event in Chile. Sci. Rep. 7, 4903. https://doi.org/10.1038/s41598-017-05123-4.
Smith, G., Askne, J., 2001. Clear-cut detection using ERS interferometry. Int. J. Remote Sens. 22, 3651–3664. https://doi.org/10.1080/01431160110040477.
Sundh, I., Nilsson, M., Mikkelä, C., Granberg, G., Svensson, B.H., 2000. Fluxes of methane and carbon dioxide on peat-mining areas in Sweden. Ambio 29, 499–503. https://doi.org/10.1579/0044-7447-29.8.499.
Tamm, T., Zalite, K., Voormansik, K., Talgre, L., 2016. Relating Sentinel-1 interferometric coherence to mowing events on grasslands. Remote Sens. 8, 802. https://doi.org/10.3390/rs8100802.
Tampuu, T., Praks, J., Uiboupin, R., Kull, A., 2020. Long term interferometric temporal coherence and DInSAR phase in Northern Peatlands. Remote Sens. 12, 1566. https://doi.org/10.3390/rs12101566.
Thiel, C.J., Thiel, C., Schmullius, C.C., 2009. Operational large-area forest monitoring in Siberia using ALOS PALSAR summer intensities and winter coherence. IEEE Trans. Geosci. Remote Sens. 47, 3993–4000. https://doi.org/10.1109/TGRS.2009.2021469.
Tissari, J.M., Yli-Tuomi, T., Raunemaa, T.M., Tiitta, P.T., Nuutinen, J.P., Willman, P.K., Lehtinen, K.E.J., Jokiniemi, J.K., 2006. Fine particle emissions from milled peat production. Boreal Environ. Res. 11, 283–293. http://www.borenv.net/BER/pdfs/ber11/ber11-283.pdf.
Touzi, R., Lopes, A., Bruniquel, J., Vachon, P.W., 1999. Coherence estimation for SAR imagery. IEEE Trans. Geosci. Remote Sens. 37, 135–149. https://doi.org/10.1109/36.739146.
Tuukkanen, T., Marttila, H., Kløve, B., 2017. Predicting organic matter, nitrogen, and phosphorus concentrations in runoff from peat extraction sites using partial least squares regression. Water Resour. Res. 53, 5860–5876. https://doi.org/10.1002/2017WR020557.
Waddington, J.M., Plach, J., Cagampan, J.P., Lucchese, M., Strack, M., 2009. Reducing the carbon footprint of Canadian peat extraction and restoration. AMBIO: A J. Hum. Environ. 38, 194–200. https://doi.org/10.1579/0044-7447-38.4.194.
Webster, K.L., Bhatti, J.S., Thompson, D.K., Nelson, S.A., Shaw, C.H., Bona, K.A., Hayne, S.L., Kurz, W.A., 2018. Spatially-integrated estimates of net ecosystem exchange and methane fluxes from Canadian peatlands. Carbon Balance Manage. 13, 16. https://doi.org/10.1186/s13021-018-0105-5.
Wegmüller, U., Werner, C., 1997. Retrieval of vegetation parameters with SAR interferometry. IEEE Trans. Geosci. Remote Sens. 35, 18–24. https://doi.org/10.1109/36.551930.
Wegmüller, U., Werner, C.L., 1995. SAR interferometric signatures of forest. IEEE Trans. Geosci. Remote Sens. 33, 1153–1161. https://doi.org/10.1109/36.469479.
Yagüe-Martínez, N., Prats-Iraola, P., González, F.R., Brcic, R., Shau, R., Geudtner, D., Eineder, M., Bamler, R., 2016. Interferometric processing of Sentinel-1 TOPS data. IEEE Trans. Geosci. Remote Sens. 54, 2220–2234. https://doi.org/10.1109/TGRS.2015.2497902.
Yu, Z., Loisel, J., Brosseau, D.P., Beilman, D.W., Hunt, S.J., 2010. Global peatland dynamics since the Last Glacial Maximum. Geophys. Res. Lett. 37 https://doi.org/10.1029/2010GL043584.
Yu, Z.C., 2012. Northern peatland carbon stocks and dynamics: a review. Biogeosciences 9, 4071–4085. https://doi.org/10.5194/bg-9-4071-2012.
Zebker, H., Villasenor, J., 1992. Decorrelation in interferometric radar echoes. IEEE Trans. Geosci. Remote Sens. 30, 950–959. https://doi.org/10.1109/36.175330.
Zwieback, S., Hensley, S., Hajnsek, I., 2015. A polarimetric first-order model of soil moisture effects on the DInSAR coherence. Remote Sens. 7, 7571–7596. https://doi.org/10.3390/rs70607571.